Rev. Roum. Sci. Techn.– Électrotechn. et Énerg.
Vol. **71**, *2*, pp. 175–180, Bucarest, 2026

SPEED SENSORLESS SLIDING MODE CONTROL FOR DUAL STAR INDUCTION MOTOR BASED ON HYBRID PSO-GWO ALGORITHM

BELGACEM HERISSI[1], AZEDDINE BEGHDADI[2], BENACHAIBA CHELLALI[3]

Keywords: Sliding mode controller; Dual star induction motor; Particle swarm grey wolf optimization (PSO-GWO); Model reference adaptive system.

This paper presents a sliding-mode model-reference adaptive system (SM-MRAS) observer for speed estimation in a sensorless, indirect vector control dual-star induction motor (DSIM) system. Firstly, a reference model of the DSIM rotor fluxes is provided using a voltage-model observer. The adjustable model adjusts the rotor flux estimates to match the reference model by adapting the speed, especially the speed estimate, which is a sliding-mode term. Secondly, the optimal parameters of the sliding mode controllers are optimized by the hybrid particle swarm grey wolf optimization (PSOGWO) algorithm. The main objective of this study is to demonstrate the effectiveness and validity of the proposed SMC-PSOGWO strategy. A comparative analysis with SMC-GWO and the conventional PI controller illustrates that the proposed method achieves a faster dynamic response and superior overall performance.

1. INTRODUCTION

Due to a significant increase in electrical energy consumption, high-power electrical applications have caused problems at the converter-machine interface. The converter switches must be switched at high current and higher switching frequencies, which necessitate the use of high-gauge components. On the other side, the machines' winding needs to be sized to withstand a high voltage [1].

To meet the mentioned criteria, Power segmentation is a suitable option for multiphase induction machines with more than three phases, driven by one or multiple converters. For this, the multi-phase machines are increasingly present in industrial applications of high power, such as railway traction, naval propulsion, and wind power systems. Among these multiphase drives, the dual star induction machines with two sets of three-phase stator windings spatially shifted by 30 electrical degrees and isolated neutral points are one of the most widely discussed topologies [2,3].

Several control strategies have been proposed for DSIM control. The two most widely used methods to control DSIM are indirect field-oriented control (IFOC) and direct torque control (DTC) [4,5]). These methods use simple PID controllers in their classic base forms to control the speed, torque, and current of the DSIM. On the other hand, these simple conventional control strategies require precise knowledge of system parameters and precise tuning of proportional-integral-derivative (PID) gains. Control laws are then developed using state feedback; their use, however, requires measurement of the state vector [5].

However, numerous difficulties arise in implementing the sensors, including sensor installation and additional costs. In order to overcome these problems, many researchers are interested in a sensorless control of induction motor drives. In (Djellouli et al. [6]), an extended Kalman filter (EKF) technique is used to estimate the speed and torque of the IM. In [7], a robust ANFIS based on the Luenberger observer has been proposed to estimate the speed and the rotor flux of the DSIM.

In [8], an artificial neural network (ANN) optimizer integrated with sensorless indirect rotor field-oriented control (IRFOC) to improve dynamic performance and efficiency in PV-powered DSIM systems. Moreover, the MRAS is a widely used machine model-based adaptive control method that requires measurements of machine operating voltages and currents to estimate speed. This method is the most attractive approach due to its design simplicity. This is the most significant advantage of MRAS over the other speed observers and is recommended for low-cost applications [9]. Recently, the sliding mode controller has been a very popular technique due to its simplicity of design and implementation, high precision, and robustness to the variation of external or internal parameters [10,11]. But the main drawback of this control technique is chattering, which causes unwanted problems and defects in the system.

Furthermore, performance degrades when the system malfunctions because the approach relies on a mathematical model of an industrial plant, and it is difficult to tune the SMC's optimal or near-optimal parameters. To solve these difficulties, many approaches have been developed in the literature to determine the parameters of SMC. In [12], a synergetic control with sliding mode extremum seeking control (SC-SMESC) has been proposed to enhance the performance and reliability of doubly fed induction generator (DFIG)-based wind turbine systems, where the SC-SMESC parameters are optimized using the PSO algorithm. In [13], the GWO and PSO algorithms were employed to optimize the sliding-mode controller to enhance reference tracking and improve the overall performance of DFIG-based wind turbine systems (WTS). Dembri et al. [14] proposed a fractional-order fuzzy proportional-integral with derivative (FOFPID) regulator to maintain the output power of the DFIG-based WTS, where the FOFPID parameters are optimized using the social spider optimization (SSO) algorithm.

The main contribution of this paper is the application of a sliding mode sensorless control scheme for a dual-star induction motor. This control strategy is used to estimate the speed to generate the switching states of the inverter and consequently the supply voltages of the DSIM. To fulfill these objectives, the optimal gains of this controller are optimized by the hybrid PSOGWO (HPSOGWO)algorithm.

2. DUAL STAR INDUCTION MACHINE MODELING

The voltages of the DSIM in the dq-reference frame are given by (Milles et al. [15]):

$$\begin{cases} V_{dqs1} = R_{s1} I_{dqs1} + \frac{\mathrm{d}\varphi_{dqs1}}{\mathrm{d}t} \mp \omega_s \varphi_{qds1}, \\ V_{dqs2} = R_{s2} I_{dqs2} + \frac{\mathrm{d}\varphi_{dqs2}}{\mathrm{d}t} \mp \omega_s \varphi_{qds2}, \\ V_{dqr} = R_r I_{dqr} + \frac{\mathrm{d}\varphi_{dqr}}{\mathrm{d}t} \mp \omega_{sr} \varphi_{qdr}, \end{cases} \quad (1)$$

[1] Department of Electronic and Telecommunication, University of Guelma, Algeria. E-mail: herissi.belgacem@univ-guelma.dz
[2] Department of Electrical Engineering, University of Sidi Bel Abbes, Algeria. E-mail: azeddine.begdadi@univ-sba.dz
[3] Department of Electrical Engineering, University of Bechar, Algeria. E-mail: benachaiba.chelali@univ-bechar.dz

DOI: 10.59277/RRST-EE.2026.2.1

where V_{dqs1}, V_{dqs2} and V_{dqr} represent the stator and rotor voltages along d and q axes, respectively; $I_{dqs1}, I_{dqs2}$and I_{dqr} are the stator and rotor currents along d and q axes, respectively; $R_{s1}, R_{s2}$and R_r are the stator and rotor resistances, respectively; $\varphi_{dqs1}, \varphi_{dqs2}$ and φ_{dqr} are the stator and rotor flux density along the d and q axes, respectively; ω_{sr} is the rotor pulsation and it is given by $\omega_{sr} = \omega_s - \omega_r$, where $\omega_s, \omega_r$are the synchronous speed and rotor speed, respectively.

The flux equations are given by:

$$\begin{cases} \varphi_{dqs1} = L_{s1} I_{dqs1} + L_m\left(I_{dqs1} + I_{dqs2} + I_{dqr}\right), \\ \varphi_{dqs2} = L_{s2} I_{dqs2} + L_m\left(I_{dqs1} + I_{dqs2} + I_{dqr}\right), \\ \varphi_{dqr} = L_r I_{dqr} + L_m\left(I_{dqs1} + I_{dqs2} + I_{dqr}\right). \end{cases} \quad (2)$$

where L_{s1}, L_{s2}, L_r and $L_m$are the stator inductances, rotor inductance, and mutual inductance, respectively.

In the DSIM, rotor windings are short-circuited, hence $V_{dqr} = 0$.

The electromagnetic torque is given by:

$$T_{em} = p\frac{L_m}{L_m + L_r}\left[\left(I_{qs1} + I_{qs2}\right)\varphi_{dr} - \left(I_{ds1} + I_{ds2}\right)\varphi_{qr}\right], \quad (3)$$

with p is the number of pole pairs.

The mechanical dynamic equation is described as:

$$\mathrm{J}\frac{\mathrm{d}\omega_r}{\mathrm{d}t} = T_{em} - T_r - K_f\omega_r, \quad (4)$$

where J is the moment of inertia, $T_r$is the load torque, and K_f is the coefficient of viscous friction.

3. MRAS-BASED SPEED-ESTIMATION TECHNIQUE

The main advantage of the MRAS method is that there is a reference model of the machine (typically a voltage model), not dependent on the rotor speed, and an adjustable model (generally a current model) depending directly on the speed [9]. The error obtained between these two models is used by an adaptation mechanism, which adjusts the adaptive model to generate an estimate of rotor speed.

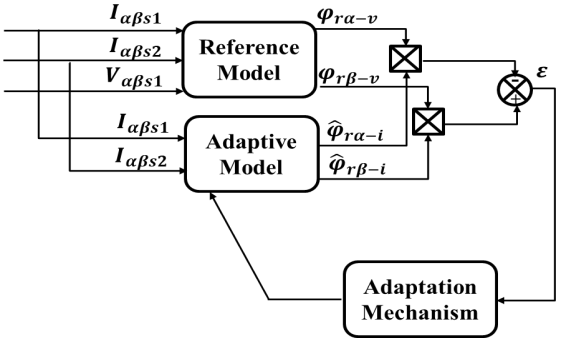

Fig. 1 – Diagram of the speed estimation structure with MRAS.

For the DSIM, the reference rotor flux components can be described by the following equations:

$$\begin{cases} \dfrac{\mathrm{d}\varphi_{r\alpha-v}}{\mathrm{d}t} = \dfrac{L_m + L_r}{L_m}\left[V_{s\alpha1} - R_{s1}i_{s\alpha1} - \right. \\ \left. \sigma(L_s + L_m)\dfrac{\mathrm{d}i_{s\alpha1}}{\mathrm{d}t} - \dfrac{L_m L_r}{L_m + L_r}\dfrac{\mathrm{d}i_{s\alpha2}}{\mathrm{d}t}\right], \\ \dfrac{\mathrm{d}\varphi_{r\beta-v}}{\mathrm{d}t} = \dfrac{L_m + L_r}{L_m}\left[V_{s\beta1} - R_{s1}i_{s\beta1} - \right. \\ \left. \sigma(L_s + L_m)\dfrac{\mathrm{d}i_{s\beta1}}{\mathrm{d}t} - \dfrac{L_m L_r}{L_m + L_r}\dfrac{\mathrm{d}i_{s\beta2}}{\mathrm{d}t}\right]. \end{cases} \quad (5)$$

The adaptive model is given by:

$$\begin{cases} \dfrac{\mathrm{d}\hat{\varphi}_{r\alpha-i}}{\mathrm{d}t} = \left[\dfrac{L_m}{T_r}\left(i_{s\alpha1} + i_{s\alpha2}\right) - \dfrac{1}{T_r}\hat{\varphi}_{r\alpha-i} - \omega_r\hat{\varphi}_{r\beta-i}\right], \\ \dfrac{\mathrm{d}\hat{\varphi}_{r\beta-i}}{\mathrm{d}t} = \left[\dfrac{L_m}{T_r}\left(i_{s\beta1} + i_{s\beta2}\right) - \dfrac{1}{T_r}\hat{\varphi}_{r\beta-i} + \omega_r\hat{\varphi}_{r\alpha-i}\right]. \end{cases} \quad (6)$$

The error for the controller is determined by the cross-product calculation:

$$\varepsilon = \varphi_{r\beta-v}\hat{\varphi}_{r\alpha-i} - \varphi_{r\alpha-v}\hat{\varphi}_{r\beta-i}. \quad (7)$$

The law of adaptation can be obtained by using a PI controller as:

$$\hat{\omega}_r = \varepsilon\left(k_p + \frac{k_i}{P}\right). \quad (8)$$

To ensure effective control of the estimation error, the MRAS adaptation mechanism is driven by a control signal generated according to the sliding mode control principle, whose detailed formulation is presented in Section 4. The SMC-based adaptation acts to regulate the MRAS estimation error and enforce convergence of the estimated speed without relying on linear PI adjustment. Furthermore, the sliding mode adaptation introduces a nonlinear corrective term into the MRAS loop, thereby reducing sensitivity to parameter variations and external disturbances compared with conventional PI-based MRAS schemes.

4. SLIDING MODE CONTROL DESIGN

Sliding mode is a type of variable structure system, it is based on a nonlinear control that uses discontinuous controls. The principal idea behind sliding mode control is to drive the state trajectory of the system towards a surface $S(X) = 0$ and maintain it around this surface with the switching logic function $U_n$given by

$$U_C = U_{eq} + U_n, \quad (9)$$

where U_{eq} and $U_n$representthe equivalent control term and discontinuous control term, respectively. The equivalent control term is calculated by solving the equation $\dot{S}(X) = 0$. It ensures stable behavior along the sliding surface.

The discrete control U_n is generally represented as a relay type, which can be expressed by equation (10) as follows:

$$U_n = K\mathrm{sign}\left(S(X)\right), \quad (10)$$

with $\mathrm{sign}\left(S(X)\right) = \begin{cases} 1 & \text{if } S > 0, \\ -1 & \text{if } S < 0. \end{cases}$

To assess the stability of the proposed sensorless control structure, the interaction between the MRAS estimation mechanism and the sliding-mode adaptation law is analyzed using a Lyapunov-based approach.

We define the speed estimation error between the actual rotor speed ω_r and its MRAS-based estimate $\hat{\omega}_r$ as

$$\varepsilon = \omega_r - \hat{\omega}_r. \quad (11)$$

The sliding surface introduced in Section 5 is expressed as

$$S(\varepsilon) = \varepsilon + \int M\varepsilon\mathrm{d}t, \ M > 0. \quad (12)$$

A Lyapunov candidate function is selected as

$$V = tS^2(\varepsilon), \quad (13)$$

which is positive definite for $S(\varepsilon) \neq 0$ and its time derivative is given by:

$$\dot{V} = S(\varepsilon)\dot{S}(\varepsilon). \quad (14)$$

By substituting the sliding-mode adaptation law developed in Section 5 into $\dot{S}(\varepsilon)$ the derivative of the

Lyapunov function becomes

$$\dot{V} = S(\varepsilon)[-k\,\mathrm{sign}(S(\varepsilon))] = -k \mid S(\varepsilon) \mid \leq 0, \quad (15)$$

where $k > 0$ is the sliding-mode gain.

But using the "sign" function often causes chattering in practice. One solution to reduce chattering is to introduce a boundary layer around the sliding surface. This is expressed by:

$$U_n = \begin{cases} k\mathrm{sgn}\big(S(x)\big) \text{ if } |S(x)| > \varepsilon, \\ \dfrac{k}{\varepsilon} S(x) if |S(x)| < \varepsilon. \end{cases} \quad (16)$$

5. SMC OF THE DUAL STAR INDUCTION MACHINE

The Sliding mode control law is designed by synthesizing a decoupled model obtained through the IFOC method [5]. The idea is to keep the error speed rotor, flux rotor, direct and quadratic stator current quantities within these sliding surfaces:

$$\begin{gathered} S(\omega_r) = \omega_r^* - \omega_r, \\ S(\varphi_r) = \varphi_r^* - \varphi_r, \\ S(I_{ds1}) = I_{ds}^* - I_{ds1}, \\ S(I_{ds2}) = I_{ds}^* - I_{ds2}, \\ S(I_{qs1}) = I_{qs}^* - I_{qs1}, \\ S(I_{qs2}) = I_{qs}^* - I_{qs2}, \end{gathered} \quad (17)$$

where the superscript $(^*)$ denotes the reference value. Accordingly, ω_r^*, φ_r^*, I_{ds}^*, and I_{qs}^*represent the reference variables of the rotor speed, flux, direct and quadratic stator current, respectively. A block diagram of sliding mode control of the DSIM is shown in Fig. 2.

The principle of the sliding mode control technique determines the control laws of the $\omega_r, \varphi_r, I_{ds}$and I_{qs} as follows:

For the speed controller

$$S(\omega_r)\dot{S}(\omega_r) < 0 \Rightarrow I_{qs}^* = I_{qseq} + I_{qsn}, \quad (18)$$

with,

$$I_{qs} = I_{qs1} + I_{qs2} \quad (19)$$

$$i_{qseq} = \frac{\mathrm{J}}{P^2}\frac{L_r+L_m}{L_m\varphi_r^*}\left[\dot{\omega}_r^* + \frac{K_f}{\mathrm{J}}\omega_r + \frac{P}{\mathrm{J}}T_r\right], \quad (20)$$

$$i_{qsn} = K_{\omega_r}\frac{S(\omega_r)}{|S(\omega_r)|+\varepsilon_{\omega_r}}. \quad (21)$$

For the flux controller

$$S(\varphi_r)\dot{S}(\varphi_r) < 0 \Rightarrow I_{ds}^* = I_{dseq} + I_{dsn}, \quad (22)$$

where,

$$I_{ds} = I_{ds1} + I_{ds2} \quad (23)$$

$$i_{dseq} = \frac{L_r+L_m}{L_m R_r}\left[\dot{\varphi}_r^* + \frac{R_r}{L_m+L_r}\varphi_r\right], \quad (24)$$

$$i_{dsn} = K_{\varphi_r}\frac{S(\varphi_r)}{|S(\varphi_r)|+\varepsilon_{\varphi_r}}. \quad (25)$$

For the stator currents controllers

$$S(I_{ds1})\dot{S}(I_{ds1}) < 0 \Rightarrow V_{ds1}^* = V_{ds1eq} + V_{ds1n}, \quad (26)$$

$$S(I_{qs1})\dot{S}(I_{qs1}) < 0 \Rightarrow V_{qs1}^* = V_{qs1eq} + V_{qs1n}, \quad (27)$$

$$S(I_{ds2})\dot{S}(I_{ds2}) < 0 \Rightarrow V_{ds2}^* = V_{ds2eq} + V_{ds2n}, \quad (28)$$

$$S(I_{qs2})\dot{S}(I_{qs2}) < 0 \Rightarrow V_{qs2}^* = V_{qs2eq} + V_{qs2n}, \quad (29)$$

with:

$$V_{ds1eq} = R_{s1}I_{ds1} + L_{s1}I_{ds1}^* - \omega_s{}^*\big(L_{s1}I_{qs1} + T_r\varphi_r{}^*\omega_{sr}{}^*\big), \quad (30)$$

$$V_{qs1eq} = R_{s1}I_{qs1} + L_{s1}I_{qs1}^* + \omega_s{}^*(L_{s1}I_{ds1} + \varphi_r{}^*), \quad (31)$$

$$V_{ds2eq} = R_{s2}I_{ds2} + L_{s2}I_{ds2}^* - \omega_s{}^*\big(L_{s2}I_{qs2} + T_r\varphi_r{}^*\omega_{sr}{}^*\big), \quad (32)$$

$$V_{qs2eq} = R_{s2}I_{qs2} + L_{s2}I_{qs2}^* + \omega_s{}^*(L_{s2}I_{ds2} + \varphi_r{}^*), \quad (33)$$

and

$$V_{ds1n} = K_{I_{ds1}}\frac{S(I_{ds1})}{|S(I_{ds1})|+\varepsilon_{I_{ds1}}}, \quad (34)$$

$$V_{qs1n} = K_{I_{qs1}}\frac{S(I_{qs1})}{|S(I_{qs1})|+\varepsilon_{I_{qs1}}}, \quad (35)$$

$$V_{ds2n} = K_{I_{ds2}}\frac{S(I_{ds2})}{|S(I_{ds2})|+\varepsilon_{I_{ds1}}}, \quad (36)$$

$$V_{qs2n} = K_{I_{qs2}}\frac{S(I_{qs2})}{|S(I_{qs2})|+\varepsilon_{I_{qs2}}}. \quad (37)$$

For the estimated speed

The control surface of the estimated speed is described as:

$$S(\varepsilon) = \varepsilon + \int M\varepsilon dt, M > 0. \quad (38)$$

The derivative of $S(\varepsilon)$is given by:

$$\dot{S}(\varepsilon) = \dot{\varepsilon} + M\varepsilon, \quad (39)$$

where,

$$\dot{\varepsilon} = A_1 - \hat{\omega}_r A_2, \quad (40)$$

with:

$$\begin{aligned} A_1 = {} & \dot{\varphi}_{r\beta-v}\hat{\varphi}_{r\alpha-i} - \dot{\varphi}_{r\alpha-v}\hat{\varphi}_{r\beta-i} \\ & + \frac{L_m}{T_r}\Big[(i_{s\alpha1} + i_{s\alpha2})\varphi_{r\beta-v} \\ & - \big(i_{s\beta1} + i_{s\beta2}\big)\varphi_{r\alpha-v}\Big] \\ & - \frac{1}{T_r}\Big[\hat{\varphi}_{r\alpha-i}\varphi_{r\beta-v} - \hat{\varphi}_{r\beta-i}\varphi_{r\alpha-v}\Big], \end{aligned} \quad (41)$$

$$A_2 = \hat{\varphi}_{r\beta-i}\varphi_{r\beta-v} + \hat{\varphi}_{r\alpha-i}\varphi_{r\alpha-v}. \quad (42)$$

By substituting (40) into (39), the derivative of the control surface can be given by:

$$\dot{S}(\varepsilon) = A_1 - \hat{\omega}_r A_2 + M\varepsilon. \quad (43)$$

Let $\hat{\omega}_r = \hat{\omega}_{req} + \hat{\omega}_{rn}$, eq. (43) can be rewritten as

$$\dot{S}(\varepsilon) = A_1 - \hat{\omega}_{req}A_2 - \hat{\omega}_{rn}A_2 + M\varepsilon. \quad (44)$$

By applying SM theory, the equivalent control $\hat{\omega}_{req}$ and attractive control $\hat{\omega}_{rn}$ takes the following forms:

$$\hat{\omega}_{req} = \frac{A_1+M\varepsilon}{A_2}, \ \hat{\omega}_{rn} = K_\varepsilon\frac{S(\varepsilon)}{|S(\varepsilon)|+\xi_\varepsilon}. \quad (45)$$

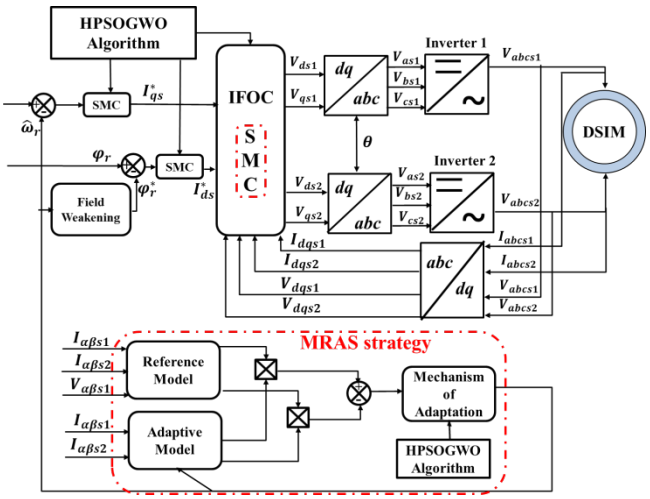

Fig. 2 – Diagram of sliding mode sensorless IFOC of the DSIM.

To calculate the sliding mode controller parameters, we used the hybrid PSOGWO algorithm.

6. GWO OPTIMIZATION OF SMC CONTROLLER

The grey wolf optimization (GWO) algorithm is a novel meta-heuristic algorithm that mimics the natural leader hierarchy and the mechanism of hunting gray wolves in the wild. The method emulates the social structure and hunting behavior in the society of gray wolves.

The grey wolf hierarchy is represented by four distinct

simulations: Alpha (α), Beta (β), Delta (δ), and Omega (ω). During the optimization process, the fitness of the solutions is evaluated and organized according to the social hierarchy of wolves, the Alpha (α) serves as the primary solution, with the Beta (β) and Delta (δ) representing the second and third-best solutions, respectively. The remaining solutions are considered least important and are assigned to the Omega group [16,17].

The following eq. (46)-(48) have been proposed to model wolf position adaptation:

$$\vec{X}_1 = \vec{X}_\alpha - \vec{A}_1(\vec{D}_\alpha), \vec{X}_2 = \vec{X}_\beta - \vec{A}_2(\vec{D}_\beta), \quad \vec{X}_3 = \vec{X}_\delta - \vec{A}_3(\vec{D}_\delta), \tag{46}$$

$$D_\alpha = |\vec{C}_1\vec{X}_\alpha - \vec{X}|, D_\beta = |\vec{C}_2\vec{X}_\beta - \vec{X}|, D_\beta = |\vec{C}_2\vec{X}_\beta - \vec{X}| \tag{47}$$

$$\vec{X}(t+1) = \frac{\vec{X}_1+\vec{X}_2+\vec{X}_3}{3}, \tag{48}$$

where X_α, X_β and X_δ are the position of α, β and δ wolves respectively, and t is the current iteration, The vectors A and C are computed as follows:

$$\begin{cases} \vec{A} = 2\vec{a}\vec{r}_1 - \vec{a}, \\ \vec{C} = 2\vec{r}_2, \end{cases} \tag{49}$$

where $\vec{a}$ is a set vector linearly decreases from 2 to 0 over iterations and r_1, r_2 are random vectors in [0 1].

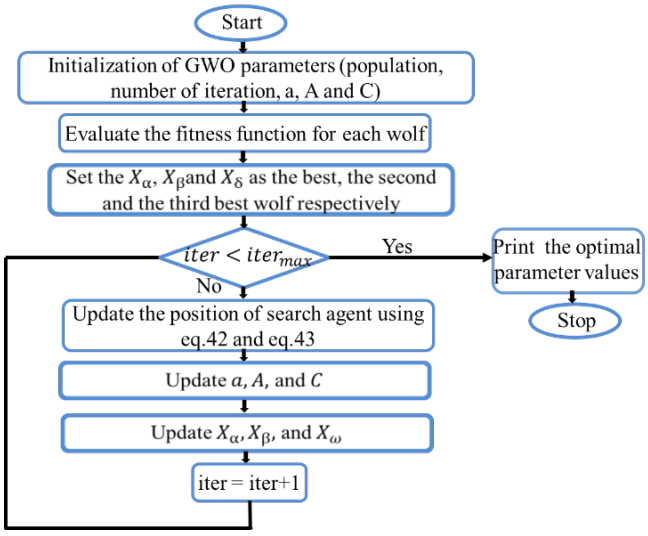

Fig. 3 – Flowchart of the GWO algorithm.

7. PARTICLE SWARM OPTIMIZATION

The particle swarm optimization algorithm is a meta-heuristic algorithm that mimics the intelligence of bird swarms, fish schools, or bee swarms. In PSO, every particle is characterized by a position vector and a velocity vector. Each particle has its own intelligence and explores a search space around the best solution that it has achieved so far. The best value achieved for all the particle's fitness functions is known as the best global $gbest$ [18]. Additionally, particles are aware of the optimal position that all of them (as a swarm) have discovered thus far. The position and velocity vectors are updated by the following expressions:

$$V_i^{k+1} = V_i^k + c_1 r_1 (Pbest_i^k - x_i^k) + c_2 r_2 (gbest - x_i^k), \tag{50}$$

$$x_i^{k+1} = x_i^k + v_i^{k+1}. \tag{51}$$

where x_i^k, v_i^k, x_i^{k+1}, and v_i^{k+1}represent the position and velocity of particle i at iterations k and $k+1$, respectively; c_1 and c_2 are the cognitive and social acceleration coefficients, respectively; r_1 and r_2 are independent random numbers uniformly distributed in [0 1]; $Pbest_i$ is the best position previously found by particle $\boldsymbol{i}$ (personal best); and $gbest$ is the best position found by the entire swarm (global best).

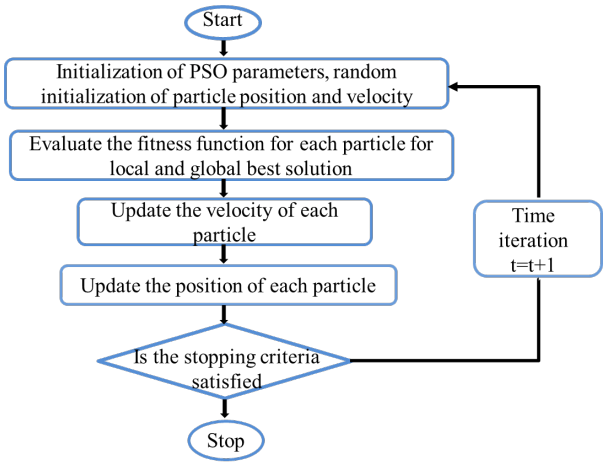

Fig. 4 – Flowchart of basic PSO algorithm.

8. THE HYBRID PSOGWO ALGORITHM

Hybrid particle swarm grey wolf optimization is a type of hybrid meta-heuristic algorithm; it is constituted by the combination of the GWO and PSO algorithms.

The principal idea behind the hybrid technique is to increase the exploitation capabilities of PSO by leveraging the exploration abilities of the GWO algorithm [19]. In this context, GWO identifies promising regions of the search space, while PSO refines the solutions based on a predefined convergence criterion. The objective of combining these abilities is to reach the global minimum faster. The mathematical model of the modified technique is given by:

$$\begin{cases} D_\alpha = |\vec{C}_1\vec{X}_\alpha - w * \vec{X}|, \\ D_\beta = |\vec{C}_2\vec{X}_\beta - w * \vec{X}|, \\ D_\delta = |\vec{C}_3\vec{X}_\delta - w * \vec{X}|. \end{cases} \tag{52}$$

To combine PSO and GWO modifications, we can define the updated velocity and positions as

$$V_i^{k+1} = w * \left(V_i^k + c_1 r_1 (x_1 - x_i^k) + c_2 r_2 (x_2 - x_i^k) + c_3 r_3 (x_3 - x_i^k)\right), \tag{53}$$

$$x_i^{k+1} = x_i^k + v_i^{k+1}. \tag{54}$$

The hybrid PSOGWO algorithm shows consistent convergence behavior, while its computational complexity is dominated by offline fitness evaluations and therefore does not affect real-time control implementation.

The PSOGWO pseudo code is as follows:

1 **Initialization**: The algorithm starts by setting parameters like population size, maximum iterations, and PSO/GWO-specific coefficients. The initial population (wolves/particles) is generated randomly, and their fitness is evaluated to identify the top three solutions (alpha, beta, delta).

2 **GWO Phase**: In each iteration, the GWO parameters controlling exploration (like A and C) are updated. The wolves adjust their positions based on the leadership hierarchy (alpha, beta, delta), simulating the hunting behavior of grey wolves.

3 **PSO Phase**: The updated positions from GWO are passed to PSO, where each particle adjusts its velocity

using its personal best and the swarm's global best. This step introduces momentum to escape local optima.

4 **Fitness Evaluation & Hierarchy Update**: New positions are evaluated, and the alpha, beta, and delta wolves are reassigned based on fitness. The loop repeats until the maximum number of iterations is reached.

5 **Termination**: The algorithm returns the best solution (alpha) as the optimal result.

9. SIMULATION RESULTS

To verify the validity of the proposed SMC-PSOGWO technique, we used MATLAB with the parameters specified in Table 1.

Table 1

Parameter of DSIM.

Rated power, P_r	4500 W
Rated voltage, V_n (Δ/Y)	220 / 380 V
Rated current, I_n	6.5 A
Rated frequency, f	50 Hz
Number of pole pairs, P	2
Stator resistance, $R_{s1} = R_{s2}$	3.72 Ω
Rotor resistance, R_r	2.12 Ω
Stator inductance, $L_{s1} = L_{s2}$	0.011 H
Rotor inductance, L_r	0.274 H
Mutual inductance, L_m	0.3672 H
Friction coefficient, K_f	0.08 N·m·s·rad^{-1}
Inertia machine, J	0.0625 kg·m^2

In the hybrid PSOGWO algorithm, the population size is fixed at 15 for both PSO particles and GWO search agents, with a maximum of 60 iterations. The PSO inertia weight decreases linearly from 0.9 to 0.4, $c_1 = c_2 = 1.75$, while the GWO control parameter a is reduced from 2 to 0.

Figure 5 shows the rotor speed response; we can remark that the speed follows its reference. This means that the speed estimation can be achieved by the proposed method.

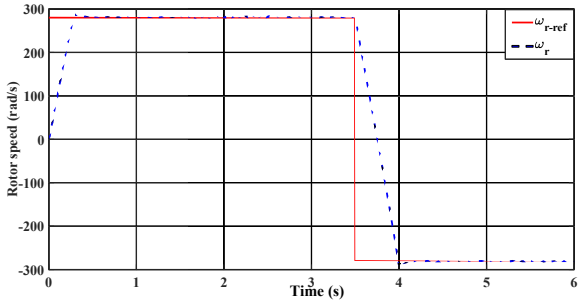

Fig. 5 – Rotor speed and its reference.

Figure 6 illustrates the response of the electromagnetic torque; we can see that the torque pursues the reference torque, which is the load torque.

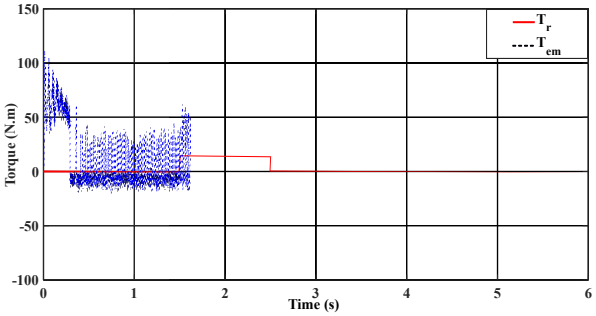

Fig. 6 – Torque.

Figure 7 shows the response of the rotor flux. The flux maintains a steady value of 1 Wb.

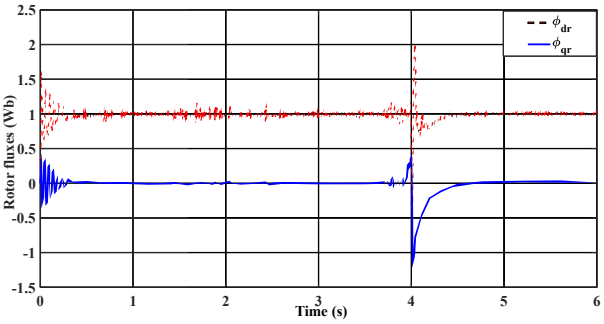

Fig. 7 – Rotor flux.

Figure 8 illustrates the stator current response; we can observe that the forms of the currents are sinusoidal with its value impacted by the variation of the load.

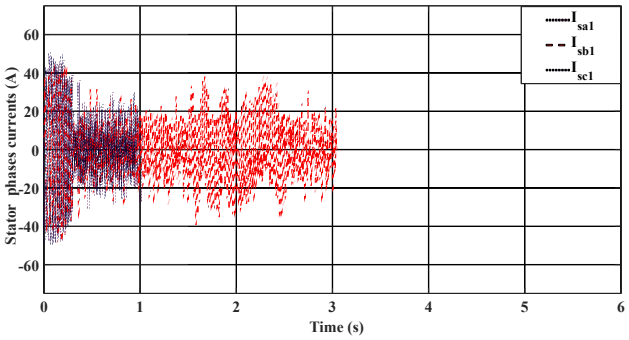

Fig. 8 – Stator current.

To demonstrate the performance of the proposed method, a comparative study with SMC-GWO and the conventional PI methods is shown in Figs. 9 and 10. The PI parameter is given by: $K_{p\omega_r} = 0.78, K_{i\omega_r} = 3.13$, $K_{p\hat{\omega}_r} = 0.56$ and $K_{i\hat{\omega}_r} = 1420$.

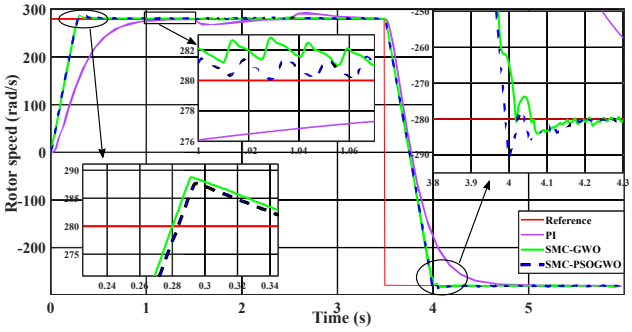

Fig. 9 – Rotor speed.

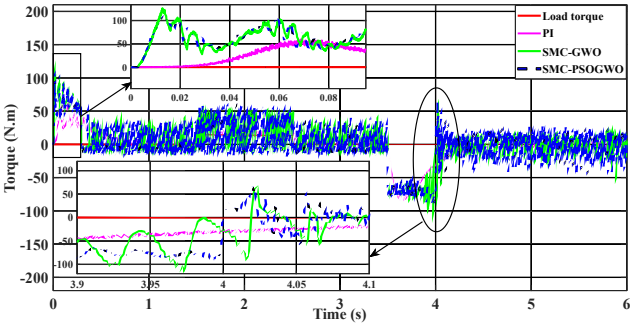

Fig. 10 – Torque.

Figures 9 and 10 show the response obtained by three methods of the rotor speed and the electromagnetic torque, respectively. The proposed SMC-PSOGWO strategy proves superior performance compared to the SMC-GWO and the traditional PI methods in terms of response time, precision, robustness, and reduction of oscillations.

10. **CONCLUSION**

This paper investigates a sliding mode-based MRAS speed estimator for a DSIM drive. By utilizing the rotor fluxes from the voltage model observer as a reference, the MRAS technique effectively adapts the speed within the current model. The proposed sensorless SMC strategy incorporates three control variables: rotor speed, rotor flux, and stator currents. To enhance dynamic performance and robustness, the controller gains are optimally tuned using a hybrid PSOGWO algorithm. Simulation results demonstrate the effectiveness of the proposed sensorless SMC compared to those obtained using both SMC–GWO and conventional PI.

Despite these improvements, certain limitations persist. In particular, the control performance is sensitive to variations in machine parameters, such as stator and rotor resistances, which may change during operation. Furthermore, the hybrid optimization approach increases the computational burden for real-time implementation. Future research will focus on developing an online parameter identification scheme to enhance robustness against thermal variations and conducting extensive experimental testing under a wider range of operating conditions. Finally, we intend to implement the algorithm to validate its industrial feasibility and extend the proposed technique to other multi-phase machine topologies.

CREDIT AUTHORSHIP CONTRIBUTION STATEMENT

BELGACEM HERISSI: conceptualization, formal analysis, methodology, investigation, visualization, writing (draft, review, and editing), validation.

AZEDDINE BEGHDADI: resources, formal analysis, investigation.

BENACHAIBA CHELLALI: supervision, investigation, validation.

Received on 5 July 2025

REFERENCES

1. K. Belalia, A. Mostefa, H. M. Boulouiha, A. Draou, M. Denai, *Direct torque control of a dual star induction generator based on a modified space vector PWM under fault conditions*, ISA Transactions, **155**, pp. 237–260 (2024).
2. I. Koussaila, T. Damak, *Field-oriented control of dual-star induction machine with energy quality based on fuzzy logic*, Rev. Roum. Sci. Techn. – Électrotechn. et Énerg., **70**, *4*, pp. 483–488 (2025).
3. R. Belal, M. Flitti, M.L. Zegai, *Tuning of PI speed controller in direct torque control of dual star induction motor based on genetic algorithms and neuro-fuzzy schemes*, Rev. Roum. Sci. Techn. – Électrotechn. et Énerg., **69**, *1*, pp. 9–14 (2024).
4. A. Kasri, K. Ouari, Y. Belkhier, D. Ziane, M.F. Benkhoris, M. Benbouzid, *Optimized voltage vector selection for dual-star induction motor: robust predictive direct torque control-based hysteresis-free approach*, ISA Transactions (2025).
5. E.S. Terfia, S. Mendaci, S.E. Rezgui, H. Gasmi, W. Kantas, *Optimal third-order sliding mode controller for dual star induction motor based on grey wolf optimization algorithm*, Heliyon, **10**, *12* (2024).
6. Y. Djellouli, S.A.E.M. Ardjoun, E. Zerdali, M. Denai, H. Chafouk, *Real-time implementation of a speed/torque sensorless observer for induction motor utilizing extended Kalman filtering technique*, 3rd International Conference on Advanced Electrical Engineering (ICAEE), Sidi-Bel-Abbes, Algeria, IEEE, November 05–07, 2024.
7. T. Roubache, S. Chaouch, *Sensorless ANFIS-based control of PV-powered double stator induction motors for EVs*, Journal Européen des Systèmes Automatisés, **57**, *1*, pp. 67–76 (2024).
8. M. Sahnoun, R. Sadouni, S. Djeriou, *Sensorless IRFOC with ANN-based speed optimization for dual-stator induction motor in photovoltaic water pumping systems*, Journal Européen des Systèmes Automatisés, **58**, *7*, pp. 1503–1512 (2025).
9. L. Zhang, R. Tao, J. Bai, D. Zeng, *An improved sliding mode model reference adaptive system observer for PMSM applications*, Expert Systems with Applications, **250**, pp. 123907 (2024).
10. C. Yang, W. Tang, Y. Sheng, Z. Zeng, *Consensus of nonlinear multiagent systems on time scales via event-triggered sliding mode control*, Journal of the Franklin Institute, **362**, *8*, pp. 107–687 (2025).
11. L. Li, C. Wang, K. Lu, Z. Wu, F. Deng, *FTUVE-based global fast terminal backstepping sliding mode control for dynamic positioning ships*, Ocean Engineering, **336**, pp. 121–709 (2025).
12. A. Khatir, A. Dida, B. Babes, F. Albalawi, Y.A. Awoke, *Particle swarm optimization of synergetic controller and sliding-mode extreme seeking controller for wind power generation system*, Scientific Reports, **15**, *1* (2025).
13. B. Ibrahim, H. Abdelkader, M.A. Hartani, K. Kayisli, *Optimization of sliding mode control for doubly fed induction generator systems using particle swarm and Grey wolf algorithms*, Electric Power Components and Systems, **52**, *10*, pp. 1782–1795 (2024).
14. R. Dembri, L. Rahmani, B. Babes, H.G. Zaini, S.S.M. Ghoneim, A.K. Bojer, A. Flah, A.B.A. Sharaf, *SSO optimized FOFPID regulator design for performance enhancement of doubly fed induction generator based wind turbine system*, Scientific Reports, **14** (2024).
15. A. Milles, E. Merabet, H. Benbouhenni, N. Debdouche, I. Colak, *Robust control technique for wind turbine system with interval type-2 fuzzy strategy on a dual star induction generator*, Energy Reports, **11**, pp. 2715–2736 (2024).
16. H. Chen, S. Q. Salih, A. Almadhor, M.N. Khan, Z. Al Barakeh, R. Ghandour, H. Albalawi et al., *Leveraging multi-effect energy utilization in a biomass-based system for H_2 production and urban energy needs: 4E analysis and ANN-based Grey Wolf optimization*, Energy, **333**, pp. 137–323 (2025).
17. Z. Liu, Z. Zhang, Q. Zhang, L. Zhao, *Prediction of landfill gases concentration based on Grey Wolf Optimization–Support Vector Regression during landfill excavation process*, Waste Management, **198**, pp. 128–136 (2025).
18. C. Diwaker, V. Hasanpuri, Y. Gulzar, B. Sharma, *Optimizing MapReduce efficiency and reducing complexity with enhanced particle swarm optimization (MR-MPSO)*, Swarm and Evolutionary Computation, **95**, pp. 101917 (2025).
19. J. Zhu, H. Qian, A. Zhu, Z. Guo, Q. Chen, Y. Xu, *Au octahedrons monolayer film SERS substrate coupled with a hybrid metaheuristic algorithm-optimized ELM model: an analytical strategy for rapid and label-free detection of zearalenone in corn oil*, Food Chemistry, **476**, pp. 143516 (2025)